Nanoscale

PAPER

View Article Online
View Journal | View Issue

Cite this: *Nanoscale*, 2024, **16**, 14096

2D petal-like PdAg nanosheets promote efficient electrocatalytic oxidation of ethanol and methanol†

Yuhua Xu,[a,b] Jie Li,[a] Mengyun Hu,[a] Zhengying Wu *[c] and Yukou Du *[a,d]

Received 8th April 2024,
Accepted 28th June 2024

DOI: 10.1039/d4nr01537a

rsc.li/nanoscale

The development of efficient alcohol electrooxidation catalysts is of vital importance for the commercialization of direct liquid fuel cells. As emerging advanced catalysts, two-dimensional (2D) noble metal nanomaterials have attracted much research attention due to their intrinsic structural advantages. Herein, we report the synthesis of petal-like PdAg nanosheets (NSs) with an ultrathin 2D structure and jagged edges *via* a facile wet-chemical approach, combining doping engineering and morphology tuning. Notably, the highly active sites and Pd–Ag composition endowed PdAg NSs with improved toxicity tolerance and substantially improved the durability toward the ethanol/methanol oxidation reaction (EOR/MOR). Moreover, the electronic effect and synergistic effect significantly enhanced the EOR and MOR activities in comparison with Pd NSs and commercial Pd/C. This work provides efficient catalysts for fuel electrooxidations and deep insight into the rational design and fabrication of novel 2D nanoarchitecture.

1. Introduction

Environmental deterioration and the urgent energy crisis call for the development of eco-friendly and renewable energy storage techniques. Direct liquid fuel cells, featuring portability, environmental friendliness, and high energy output, hold great potential as future possible energy substitutes.[1–4] Methanol and ethanol possess many advantages as excellent liquid fuels including high volume energy density and ready availability.[4–6] Therefore, direct alcohol fuel cells (DAFC) and direct methanol fuel cells (DMFC) have gained widespread attention in recent years. However, the sluggish ethanol and methanol oxidation reaction (EOR and MOR) kinetics remain a severe challenge.[7–9] Previous studies have demonstrated that Pd-based nanomaterials are favorable electrocatalysts for EOR and MOR.[10–12] Nonetheless, conventional Pd-based catalysts suffer from insufficient activity and poor operation durability, which still hinder their further utilization. Therefore, designing and synthesizing active and durable Pd-based catalysts is highly desired.

It has been demonstrated that the catalytic behavior depends on the surface structure, involving the composition, morphology, and electronic states. Generally, alloying Pd with other metals, *e.g.* Au, Ag,[13,14] or nonmetals, *e.g.* P, S, has been regarded as an efficient strategy to improve the atom utilization of Pd and tune the surface structure.[15] The doping of foreign elements induces electron redistribution and modifies the electronic structure of Pd, thereby enhancing the antipoisoning ability of Pd-based nanomaterials. Moreover, the synergistic effect between Pd and foreign elements also contributes to boosting the reaction kinetics toward fuel oxidation.[16–20] Therefore, rational composition tuning in Pd-based nanomaterials is of great significance to catalytic performance enhancement.

Apart from doping engineering, tuning the morphology of the alloy nanostructures offers great flexibility to optimize electrocatalytic performance yet it remains challenging in terms of synthesis and mechanism exploration. Among various dimension nanostructures, 2D Pd-based nanomaterials are considered a kind of high-performance catalyst for anodic reactions.[21–23] Previous advances proposed that precise structural regulation on 2D nanomaterials could afford rich active sites for anodic reactions. For instance, Wang and co-worker reported that edge engineering for 2D PdPtCu nanostructures and the ample edge sites of nanosheets and nanorings accounted for the excellent EOR performances.[24] It was found that low-coordinated edge sites were more vigorous to

[a]*College of Chemistry, Chemical Engineering and Materials Science, Soochow University, Suzhou 215123, China. E-mail: duyk@suda.edu.cn*
[b]*The School of Science, Xi'an Jiaotong-Liverpool University, Suzhou 215028, China*
[c]*Jiangsu Key Laboratory for Environment Functional Materials, School of Materials Science and Engineering, Suzhou University of Science and Technology, Suzhou 215009, China. E-mail: zywu@mail.usts.edu.cn*
[d]*School of Optical and Electronic Information, Suzhou City University, Suzhou 215104, PR China*

† Electronic supplementary information (ESI) available. See DOI: https://doi.org/10.1039/d4nr01537a

substantially improve the total catalytic efficiency.[25–29] This work has inspired a strategy of constructing 2D Pd-based nanostructures with highly active sites to realize excellent catalytic performance toward EOR and MOR.

Based on the considerations above, we adopted a facile wet-chemical reduction for fabricating petal-like PdAg nanosheets (NSs) with jagged edges. The doping of Ag endows PdAg NSs with a robust electronic effect and bimetallic synergy, achieving improved toxicity tolerance and thus exhibiting remarkable catalytic performance. Noticeably, the unique jagged edges give catalysts highly active sites with high surface energy, which could favor the adsorption and activation of fuel molecules. Consequently, the as-obtained PdAg NSs exhibit mass activities of 4.5 and 1.3 A mg^{-1} for the EOR and MOR, which are 5.0 and 4.1 times that of commercial Pd/C, respectively. This work provides a reference for the rational design of elaborate 2D Pd-based nanostructures with highly active sites.

2. Results and discussion

2.1. Physical characterization of PdAg NSs

2D PdAg NSs with distinct petal-like structures were fabricated using a facile wet-chemistry approach, based on the thermal decomposition of sodium tetrachloropalladate and the reduction of silver nitrate in a mixed solvent of benzyl alcohol and acetylacetone. In the one-pot synthesis route, cetyltrimethylammonium chloride and molybdenum carbonyl were also employed as structure-directed and reducing agents, respectively. As shown in Fig. 1a and b, the high-angle annular dark-field scanning transmission electron microscopy (HAADF-STEM) and low-resolution TEM images reveal that the well-dispersed PdAg NSs exhibit a high yield approaching 100% and a 2D ultrathin nanoarchitecture. A lattice fringe of 0.230 nm can be observed (Fig. 1c), corresponding to the lattice distance of the (111) plane for the cubic Pd phase in a high-resolution TEM image. Moreover, the unique PdAg NSs possessed numerous low-coordinated sites at the jagged edges (Fig. 1d), which could be beneficial for catalytic performance enhancement. As shown in Fig. S1,† the high-quality nanosheets exhibited an average thickness and lateral size of about 2.2 nm and 96.4 nm, respectively.

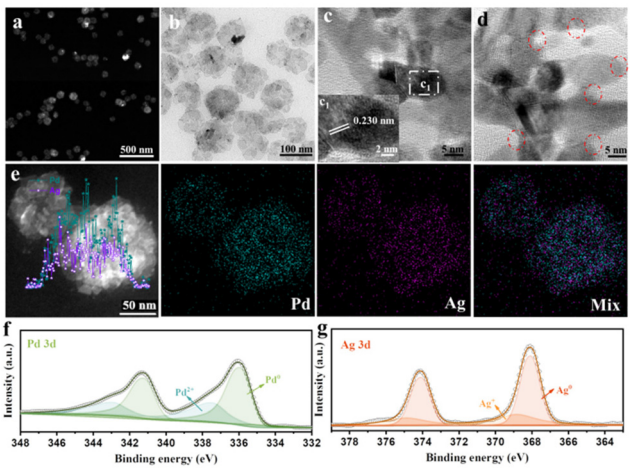

Fig. 1 (a) HAADF-STEM image, (b) TEM image, (c and d) high-magnification TEM images, (e) HAADF-STEM-EDS elemental mappings; inset of line-scan analysis, (f) Pd 3d and (g) Ag 3d XPS spectra of $PdAg_{1.5}$ NSs.

Selected-area electron diffraction (SAED) and X-ray diffraction (XRD) were performed to further reveal the structural features. Multiple diffraction rings in the SAED pattern confirmed the polycrystalline structure of PdAg NSs (Fig. S2†). Compared with the standard face-centered cubic Pd structure, the peak positions of PdAg NSs were left-shifted to lower degrees, originating from the doping of Ag into the Pd lattice for the formation of PdAg alloy (Fig. S3†). AgCl impurity was observed in the XRD pattern, which originated from the metal precursor and was electrochemically inactive. HAADF-STEM-energy-dispersive X-ray spectroscopy (EDS) demonstrated the uniform merging of Pd and Ag elements in the nanosheets, being consistent with the line-scan analysis inset in Fig. 1e.

For comparison, 2D Pd NSs with smooth edges were synthesized as a reference (Fig. S4†). X-ray photoelectron spectroscopy (XPS) was carried out to investigate the electronic structure of PdAg and Pd NS catalysts. As shown in Fig. 1f and Fig. S5,† they exhibited two sets of peaks of Pd 3d orbitals, corresponding to metallic Pd and of Pd^{2+} species. Notably, a noticeable increase in metallic Pd was observed after the doping of Ag, which was revealed by the increase in the integrated area ratio of Pd^0/Pd^{2+} from 0.29 to 0.53. It was found that the incorporation of Ag tailored the metal interaction, resulting in a robust electronic effect for catalytic performance optimization. Fig. 1g shows that Ag mainly exists in the metallic state on the surface of PdAg NSs. The above analyses demonstrate that doping engineering and morphology tuning can realize the optimization of electrocatalysts in terms of surface, geometry, and electronic structures, so that the PdAg NSs are expected to deliver excellent performance.

The intermediate products collected at different reaction stages were used to reveal the time-dependent composition, shape evolution, and phase structures of the petal-like PdAg NSs during the synthesis process. As shown in Fig. 2a–d, metal precursors were rapidly reduced simultaneously, forming a unique 2D structure due to the similar reduction potentials between Ag^+/Ag and $[PdCl_4]^{2-}/Pd$.[30] After being heated for 5–25 min, the composition evolved from a Pd/Ag of 84.7/15.3 to 71.4/28.6 (Fig. S6†). The XRD patterns demonstrated that the increase in Ag content made the diffraction peak shift to the low angle region, indicating an increased alloying degree (Fig. 2f).[31] Furthermore, the effects of the presence of PVP, CTAC, and $Mo(CO)_6$ on the nanosheet formation were investigated. It is well known that PVP serves as a surface coating to stabilize the nanosheets against agglomeration. Synthesis in the absence of CTAC yielded plate-like nanostructures with inhomogeneous shapes (Fig. S7a and b†). The results suggested that CTAC played an important role in the preferential growth of 2D petal-like PdAg nanosheets. The reported works have proposed that selective bonding of halide ions on

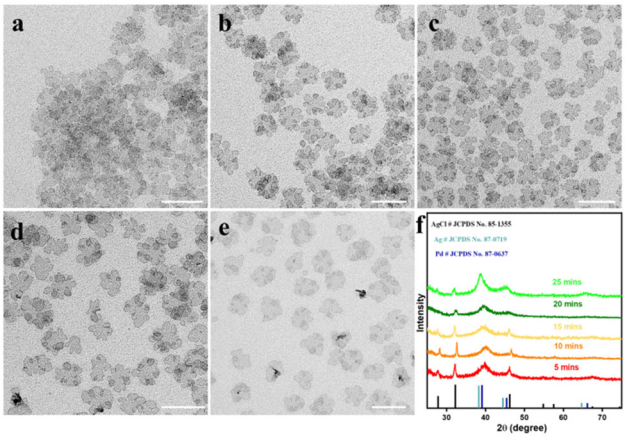

Fig. 2 TEM images of $PdAg_{1.5}$ NS intermediate products collected at (a) 5 min, (b)10 min, (c) 15 min, (d) 20 min, and (e) 25 min. The bars in (a)–(e) are 100 nm. (f) The corresponding XRD patterns of different intermediate products.

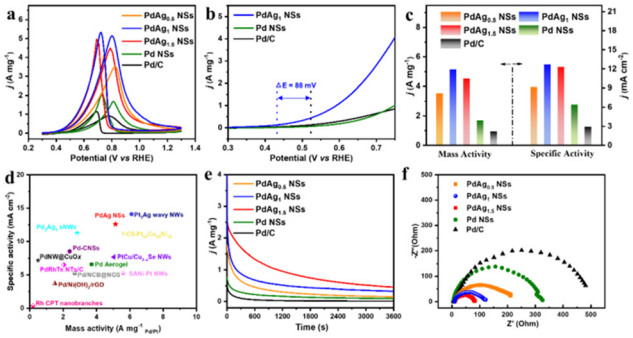

Fig. 3 (a) CV curve in 1 M KOH + 1 M ethanol solution, (b) onset potential (c) mass and specific activity, (d) performance comparison of different catalysts toward the EOR, (e) CA tests, and (f) Nyquist plots of $PdAg_{0.5}$ NS, $PdAg_1$ NS, $PdAg_{1.5}$ NS, Pd NS, and Pd/C catalysts.

(100) of fcc metals can regulate the lateral growth rate and thus is essential for the formation of a homogeneous shape for the nanomaterials. Furthermore, synthesis in the absence of $Mo(CO)_6$ yielded nanoplates with ill-defined structures (Fig. S7c and d†). The CO in the $Mo(CO)_6$, serving as a surface confining agent, has previously been demonstrated and applied for the preparation of ultrathin Pd-based nanosheets.

2.2. Electrochemical performance of catalysts

Other PdAg NSs were also prepared by changing the amounts of $AgNO_3$ and PdAg NSs with different Pd/Ag ratios all exhibiting a 2D petal-like nanostructure (Fig. S8†). The EOR and MOR activities of PdAg NSs were evaluated and benchmarked against the Pd NSs and commercial Pd/C. Before the electrochemical tests, the as-prepared PdAg and Pd NSs were loaded on carbon black (Vulcan XC72R carbon, C) for subsequent tests. The cyclic voltammograms (CVs) of different catalysts were recorded with a sweep rate of 50 mV s^{-1} in 1 M KOH electrolyte. Based on the reduction charges of PdO in CVs, the electrochemical active surface areas (ECSAs) for $PdAg_{0.5}$ NSs, $PdAg_1$ NSs, $PdAg_{1.5}$ NSs, Pd NSs, and Pd/C were calculated to be 38.8, 40.7, 36.7, 26.6 and 31.7 m^2 g^{-1}, respectively (Fig. S9†).

The PdAg and Pd NSs were first employed as anodic MOR electrocatalysts. Fig. 3a presents the CVs of all catalysts in 1 M KOH solution containing 1 M ethanol. As depicted in Fig. 3, $PdAg_1$ NSs exhibited the highest forward current among these catalysts, indicating better EOR activity. Moreover, the onset potential of $PdAg_1$ NSs was much more negative than those of commercial Pd/C and Pd NSs by 88 mV (Fig. 3b), for which reason the doping of Ag and highly active sites at the jagged surface could contribute to improving the anodic reaction kinetics. The mass and specific activity of different catalysts are summarized in Fig. 3c by normalizing the peak current in the forward scan with the loaded amount of Pd and ECSA. The $PdAg_1$ NSs delivered a mass activity of 5.1 A mg^{-1}, which was 6.1, 3.0, 1.5, and 1.1 times higher than those of Pd/C (0.9 A mg^{-1}), Pd NS (1.7 A mg^{-1}), $PdAg_{0.5}$ NS (3.5 A mg^{-1}), and $PdAg_{1.5}$ NS (4.5 A mg^{-1}) catalysts, respectively. As for the specific activity, $PdAg_1$ NSs also exhibited the highest specific activity of 12.6 mA cm^{-2}, which was far beyond those of Pd/C and Pd NSs. These petal-like PdAg NSs presented excellent electrooxidation activity, even greater than the values for various reported catalysts toward EOR (Fig. 3d). The electrochemical durability of various catalysts was investigated by chronoamperometric (CA) tests and CV cycling. These PdAg NSs maintained much higher mass activity over the entire course in comparison with Pd NSs and Pd/C (Fig. 3e), revealing their remarkable long-term stability. Consecutive CVs were carried out to further investigate the electrocatalytic durability. After 250 cycles, the highest mass activity was observed on $PdAg_1$ NS catalysts during the whole testing program (Fig. S10†). In addition, electrochemical impedance spectra (EIS) were employed to evaluate the capability of electron transport in different catalysts (Fig. 3f). In Nyquist plots, the semicircular diameters for these PdAg NSs were much smaller than those of Pd NSs and Pd/C, indicating that the incorporation of Ag can significantly promote electron transport for the EOR.[32,33]

Furthermore, we evaluated the anodic MOR performances of different catalysts. Fig. 4a shows the typical MOR anodic scan curves in 1 M KOH solution containing 1 M methanol. As depicted in Fig. 4a, the 2D $PdAg_1$ NSs delivered the highest mass activity from 0.6 to 1.0 V *vs* a reversible hydrogen electrode (RHE) among all the catalysts. The lowest onset potential was observed on the $PdAg_1$ NS surface, which was more negative than those of Pd/C and Pd NSs by 150 mV (Fig. 4b), implying facilitated catalytic efficiency. The mass activity of the $PdAg_1$ NSs was determined to be 1.5 A mg^{-1} (Fig. 4c), which was 5.0-fold, 2.5-fold, 1.4-fold, and 1.2-fold larger than those of Pd/C (0.3 A mg^{-1}), Pd NS (0.6 A mg^{-1}), $PdAg_{0.5}$ NS (1.1 A mg^{-1}), and $PdAg_{1.5}$ NS (1.3 A mg^{-1}) catalysts, respectively. Accordingly, $PdAg_1$ NSs exhibited a specific activity of 3.6 mA cm^{-2}, 3.6-fold, and 1.7-fold larger than those of Pd/C and Pd NSs, respectively. As summarized in Fig. 4d, the construction

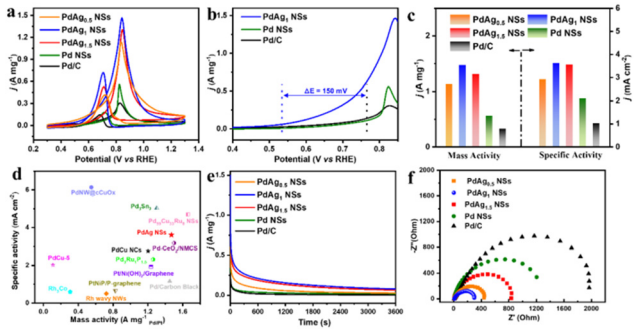

Fig. 4 (a) CV curve in 1 M KOH + 1 M methanol solution, (b) onset potential (c) mass and specific activity, (d) performance comparison of different catalysts toward the MOR, (e) CA tests, and (f) Nyquist plots of $PdAg_{0.5}$ NS, $PdAg_1$ NS, $PdAg_{1.5}$ NS, Pd NS, and Pd/C catalysts.

of PdAg materials with jagged surfaces and 2D ultrathin nanostructures make it a good noble-based electrocatalyst toward the MOR. Among all the as-prepared electrocatalysts, the $PdAg_1$ NSs maintained the highest mass activity for CA tests after 3600 s (Fig. 4e), which matched well with the results observed in their 250 CV cycling (Fig. S11†). Similarly, the unique structure endowed PdAg NSs with better capacity for electron transport during the MOR process over Pd NSs and Pd/C (Fig. 4f).

It is well known that Pd is very susceptible to CO poisoning. Therefore, CO-stripping tests were carried out to evaluate the CO tolerance of catalysts. As depicted in Fig. S12,† the $PdAg_1$ NS catalyst exhibited the most negative onset potential compared to Pd NSs and commercial Pd. The negative shift in CO-stripping onset potential for $PdAg_1$ NSs indicated the weakened adsorption energy of carbonaceous intermediates, which agreed well with the improved CO tolerance and electrocatalytic activity from the experimental observations. The enhanced CO tolerance sustainably improved the electrocatalytic activity and stability. Consequently, the incorporation of Ag modified the electronic structure of Pd, therefore weakening the affinity for carbonaceous poisonous species through synergistic effects and electronic effects.

In addition, PdAg NSs after the durability tests showed relatively limited changes with the 2D ultrathin structure (Fig. S13†), while the commercial Pd/C exhibited serious aggregation (Fig. S14†), further confirming the enhanced structural stability. In comparison with the zero-dimensional (0D) Pd/C catalyst, the superior stability of PdAg NSs could originate from the anisotropic morphology. To be more specific, the 2D nanostructure and the jagged edges endowed catalysts with high surface area and highly active sites, facilitating the adsorption and activation of reaction molecules and subsequent oxidation of carbonaceous intermediates.[34–36] On the other hand, 2D PdAg NSs can effectively strengthen the interaction between NSs and the carbon support, which is beneficial for improving the chemical stability and boosting catalysis.[37,38]

3. Conclusions

In summary, we demonstrated the synthesis of the petal-like PdAg NSs through a facile wet-chemistry approach. This unique material featured an ultrathin 2D nanostructure and jagged edges, acting as a promising electrocatalyst for the anodic fuel oxidation reaction. The as-obtained PdAg NSs presented excellent electrocatalytic activity and durability, as well as enhanced reaction kinetics, which are superior to those of Pd NS and Pd/C catalysts for the EOR/MOR. Detailed investigations confirmed that the remarkable catalytic properties could be attributed to the tailored electronic structure, fast electron transport, and synergistic effect between Pd and Ag originating from doping engineering. Moreover, the morphology tuning provided highly active sites, and sustainably activated the adsorption and activation of fuel molecules, resulting in robust resistance to toxicity and improved long-term durability of the well-organized PdAg NSs. This work presents a new understanding of the jagged edge in a 2D alloy nanostructure, improving the design of efficient electrocatalysts for fuel cell catalysis.

Author contributions

Yuhua Xu: Conceptualization, methodology, investigation, writing – original draft. Jie Li: Conceptualization, methodology, investigation, writing – original draft. Mengyun Hu: Writing – review & editing. Zhengying Wu: Supervision, resources. Yukou Du: Resources, supervision, funding acquisition.

Data availability

The data that support the findings of this study are available from the corresponding author, YD, upon reasonable request.

Conflicts of interest

There are no conflicts to declare.

Acknowledgements

This work was supported by the National Natural Science Foundation of China (grant numbers 52274304, 52073199).

References

1 X. Wang, M. Xie, F. Lyu, Y.-M. Yiu, Z. Wang, J. Chen, L.-Y. Chang, Y. Xia, Q. Zhong, M. Chu, H. Yang, T. Cheng, T.-K. Sham and Q. Zhang, *Nano Lett.*, 2020, **20**, 7751–7759.
2 Q. Yun, Y. Ge, Z. Shi, J. Liu, X. Wang, A. Zhang, B. Huang, Y. Yao, Q. Luo, L. Zhai, J. Ge, Y. Peng, C. Gong, M. Zhao,

Y. Qin, C. Ma, G. Wang, Q. Wa, X. Zhou, Z. Li, S. Li, W. Zhai, H. Yang, Y. Ren, Y. Wang, L. Li, X. Ruan, Y. Wu, B. Chen, Q. Lu, Z. Lai, Q. He, X. Huang, Y. Chen and H. Zhang, *Chem. Rev.*, 2023, **123**, 13489–13692.
3 Y. Yang, M. Luo, W. Zhang, Y. Sun, X. Chen and S. Guo, *Chem*, 2018, **4**, 2054–2083.
4 X. Yang, Q. Yuan, T. Sheng and X. Wang, *Chem. Sci.*, 2024, **15**, 4349–4357.
5 W. Huang, X.-Y. Ma, H. Wang, R. Feng, J. Zhou, P. N. Duchesne, P. Zhang, F. Chen, N. Han, F. Zhao, J. Zhou, W.-B. Cai and Y. Li, *Adv. Mater.*, 2017, **29**, 1703057.
6 J. Li, Y. Xu, C. Wang, Z. Wu, Y. Shiraishi and Y. Du, *Surf. Interface*, 2023, **42**, 103360.
7 H. Peng, J. Ren, Y. Wang, Y. Xiong, Q. Wang, Q. Li, X. Zhao, L. Zhan, L. Zheng, Y. Tang and Y. Lei, *Nano Energy*, 2021, **88**, 106307.
8 Y. Li, P. Kidkhunthod, Y. Zhou, X. Wang and J. M. Lee, *Adv. Funct. Mater.*, 2022, **32**, 2205985.
9 H. Jin, X. Wei, L. Zhao, J. Yu, Q. Pan, S. Li, Q. Wang, Z. Yuan, D. Yang, D. Zhao, H. Chen and Y. Wang, *Nano Res.*, 2024, **17**, 3334–3343.
10 J. Xue, Z. Hu, H. Li, Y. Zhang, C. Liu, M. Li, Q. Yang and S. Hu, *Nano Res.*, 2022, **15**, 8819–8825.
11 L. Jin, H. Xu, C. Chen, H. Shang, Y. Wang, C. Wang and Y. Du, *ACS Appl. Mater. Interfaces*, 2019, **11**, 42123–42130.
12 F. Zhao and Q. Yuan, *Inorg. Chem.*, 2023, **62**, 14815–14822.
13 F. Lv, W. Zhang, M. Sun, F. Lin, T. Wu, P. Zhou, W. Yang, P. Gao, B. Huang and S. Guo, *Adv. Energy Mater.*, 2021, **11**, 2100187.
14 X. Fu, C. Wan, A. Zhang, Z. Zhao, H. Huyan, X. Pan, S. Du, X. Duan and Y. Huang, *Nano Res.*, 2020, **13**, 1472–1478.
15 J. Liu, Z. Luo, J. Li, X. Yu, J. Llorca, D. Nasiou, J. Arbiol, M. Meyns and A. Cabot, *Appl. Catal., B*, 2019, **242**, 258–266.
16 Y. Qin, H. Huang, W. Yu, H. Zhang, Z. Li, Z. Wang, J. Lai, L. Wang and S. Feng, *Adv. Sci.*, 2022, **9**, 2103722.
17 M. Luo, Z. Zhao, Y. Zhang, Y. Sun, Y. Xing, F. Lv, Y. Yang, X. Zhang, S. Hwang, Y. Qin, J.-Y. Ma, F. Lin, D. Su, G. Lu and S. Guo, *Nature*, 2019, **574**, 81–85.
18 M. Farsadrooh, J. Torrero, L. Pascual, M. A. Peña, M. Retuerto and S. Rojas, *Appl. Catal., B*, 2018, **237**, 866–875.
19 J. Li, C. Wang, Y. Zhang, S. Hata, K. Zhang, C. Ye, Y. Shiraishi and Y. Du, *J. Energy Chem.*, 2023, **85**, 430–438.
20 X. Yang, Q. Yuan, J. Li, T. Sheng, K. X. Yao and X. Wang, *Nano Lett.*, 2023, **23**, 3467–3475.
21 Z. Lyu, X.-G. Zhang, Y. Wang, K. Liu, C. Qiu, X. Liao, W. Yang, Z. Xie and S. Xie, *Angew. Chem., Int. Ed.*, 2021, **60**, 16093–16100.
22 G. Wu, X. Han, J. Cai, P. Yin, P. Cui, X. Zheng, H. Li, C. Chen, G. Wang and X. Hong, *Nat. Commun.*, 2022, **13**, 4200.
23 Z. Lin, B. Xiao, Z. Wang, W. Tao, S. Shen, L. Huang, J. Zhang, F. Meng, Q. Zhang, L. Gu and W. Zhong, *Adv. Funct. Mater.*, 2021, **31**, 2102321.
24 W. Wang, X. Zhang, Y. Zhang, X. Chen, J. Ye, J. Chen, Z. Lyu, X. Chen, Q. Kuang, S. Xie and Z. Xie, *Nano Lett.*, 2020, **20**, 5458–5464.
25 H. Luo, K. Wang, F. Lin, F. Lv, J. Zhou, W. Zhang, D. Wang, W. Zhang, Q. Zhang, L. Gu, M. Luo and S. Guo, *Adv. Mater.*, 2023, **35**, 2211854.
26 M. Jin, S. Liu, G. Meng, S. Zhang, Q. Liu, J. Luo and X. Liu, *Adv. Mater. Interfaces*, 2023, **10**, 2201144.
27 X. Wang, J. Li, X. Yang, F. Zhao, Y. Li, D. Zhang, L.-Y. Gan, K. X. Yao and Q. Yuan, *Nano Res.*, 2022, **15**, 7951–7958.
28 J. Li, Z. Zhou, H. Xu, C. Wang, S. Hata, Z. Dai, Y. Shiraishi and Y. Du, *J. Colloid Interface Sci.*, 2022, **611**, 523–532.
29 Y. Yan, X. Li, M. Tang, H. Zhong, J. Huang, T. Bian, Y. Jiang, Y. Han, H. Zhang and D. Yang, *Adv. Sci.*, 2018, **5**, 1800430.
30 H. Lv, Y. Wang, A. Lopes, D. Xu and B. Liu, *Appl. Catal., B*, 2019, **249**, 116–125.
31 Y. Zhang, B. Huang, Q. Shao, Y. Feng, L. Xiong, Y. Peng and X. Huang, *Nano Lett.*, 2019, **19**, 6894–6903.
32 S. Bai, Y. Xu, K. Cao and X. Huang, *Adv. Mater.*, 2021, **33**, 2005767.
33 Y. Bao, H. Liu, Z. Liu, F. Wang and L. Feng, *Appl. Catal., B*, 2020, **274**, 119106.
34 F. Lin, F. Lv, Q. Zhang, H. Luo, K. Wang, J. Zhou, W. Zhang, W. Zhang, D. Wang, L. Gu and S. Guo, *Adv. Mater.*, 2022, **34**, 2202084.
35 W. Zhu, L. Zhang, P. Yang, C. Hu, Z. Luo, X. Chang, Z.-J. Zhao and J. Gong, *Angew. Chem., Int. Ed.*, 2018, **57**, 11544–11548.
36 J. Ding, F. Wang, F. Pan, P. Yu, N. Gao, R. H. Goldsmith, S. Cai, R. Yang and J. He, *ACS Catal.*, 2021, **11**, 13721–13732.
37 Z. Huang, S. Li, B. Xu, F. Yan, G. Yuan and H. Liu, *Small*, 2021, **17**, 2006624.
38 Y. Zhao, X. Tan, W. Yang, C. Jia, X. Chen, W. Ren, S. C. Smith and C. Zhao, *Angew. Chem., Int. Ed.*, 2020, **59**, 21493–21498.